Prediction of Surface Topography of Laser Interference Textured Steel Using Machine Learning and Surfalize

Frederic Schell*1, Christoph Zwahr1, and Andrés F. Lasagni1,2

¹Fraunhofer Institute for Material and Beam Technology IWS, Winterbergstr. 28, 01277 Dresden, Germany

²Technische Universität Dresden, Institut für Fertigungstechnik, Georg-Bähr-Str. 3c, 01069 Dresden, Germany

*Corresponding author's e-mail: frederic.schell@iws.fraunhofer.de

Understanding how laser process parameters influence surface topography is crucial for precise laser surface texturing. While the complex relationship between laser process and topographical parameters is difficult to model analytically, it lends itself well to machine learning. The requirement for large datasets of topographic parameters has generated a need for software solutions based in Python and equipped with batch functionality. In this work, we demonstrate the application of the self-developed Python library Surfalize to analyze a large dataset of direct laser interference patterning textured surfaces in terms of roughness parameters and train different machine learning models to predict topographical features from process parameters. The results show that both the random forest regressors and gradient boost machines exhibit the best predictive accuracy across a wide range of parameters, reaching R^2 values above 0.9 for amplitude related features such as the structure depth and arithmetic mean height. On the other hand, k-nearest neighbors and support vector machines perform significantly worse. Moreover, parameters from the functional family are predicted with less accuracy than amplitude or hybrid parameters.

DOI: 10.2961/ilmn.2025.03.2001

Keywords: laser texture, surface roughness, topography, prediction, machine learning, surfalize

1. Introduction

Laser surface texturing, particularly using the direct laser interference patterning (DLIP) technique, has garnered significant attention in recent years due to its manifold applications in areas such as controlling wetting [1,2], biocompatibility and cell behavior [3,4], optical [5,6] and tribological [7,8] properties. Many of these applications often require specific surface geometries, often defined by the spatial period, peak-to-valley and surface roughness of the pattern to achieve an optimal effect. However, the surface topographies of structures that are obtained by laser processing is highly dependent on a large number of parameters, encompassing both the process parameters such as the utilized pulse energy, repetition rate, scan speed and hatch distance, as well as the machine-specific settings. The machine specific settings encompass factors such as the laser source's pulse duration and wavelength, the exact beam profile, the employed focal length, the precision and vibrations in the positioning system. On the other hand, the resulting topography can be quantified with a wide range of metrics, such as the roughness values defined in ISO 25178 [9], which play a key role to determine the surface functionality.

The function linking the process to the topography parameters presents a high-dimensional and complex relationship, which is difficult to model analytically, even though some attempts have been made using semi-empirical models [10] as well as design of experiments approaches [11]. In order to accurately predict the surface topography from the process parameters, this function has to be known. However,

with the widespread rise of machine learning and increase of computing power, these relationships can now be modeled without understanding its complex nature.

For direct laser writing (DLW) techniques, some research works have already applied machine learning to predict surface topography from process parameters. For instance, Steege et al. [12] used random forest regressors (RFR) and artificial neural networks to predict surface roughness of DLW produced surface textures. Moles et al. [13] compared six different machine learning models for the prediction of femtosecond laser grooves and could also apply an inverse approach to obtain prediction of laser parameters for a given input geometry. Moreover, in laser powder bed fusion, machine learning is already extensively applied to predict and optimize process parameters and material properties [14–16]. However, to the best of the authors' knowledge, it has not yet been applied to DLIP.

A common problem in machine learning is the acquisition of a large enough dataset. For surface topography evaluation, the bottleneck is often the measurement, topographic post-processing and evaluation of the laser textures by proprietary software packages, while the machine learning pipeline itself is typically realized in Python. We tackle this problem by using applying the self-developed Python library Surfalize to post-process and evaluate the topographical data. The library is open-source, offers common roughness parameters from ISO 25178 [9] as well as batch functionality for rapid evaluation of large datasets and is described in detail in [17].

In this work, we demonstrate an application of Surfalize for use in machine learning to predict surface roughness in DLIP processing. A large dataset of DLIP textures is analyzed, and various machine learning models are trained to predict topography based on process parameters. Their performance is compared in respect to each other and across different families of topographical parameters.

2. Materials and Methods

2.1 Materials

The DLIP textures were fabricated on samples made from tool steel 1.4301. The untextured surface exhibited relatively high arithmetic mean height (S_a) values of 0.6 μ m and had an anisotropic roughness profile as a result of the machining finish.

2.2 Laser texturing

The textures were fabricated using a DLIP optical configuration with a diffractive optical element (DOE) that splits the beam into two sub-beams corresponding to the first diffraction orders and a biprism that parallelizes them at an adjustable distance from the DOE. The parallel beams are overlapped on the substrate surface by an aspheric converging lens with a focal length of 100 mm, resulting in an interference angle that depends solely on the distance of the parallel beams, which in turn is controlled by changing the distance of the biprism from the DOE. The resulting spatial period (Λ) of the line-like interference pattern depends on the laser wavelength and the angle (θ) between the beams as follows:

$$\Lambda = \frac{\lambda}{2\sin(\frac{\theta}{2})}. (1)$$

The DLIP optical setup was combined with both a nanosecond and picosecond pulsed laser sources. The nanosecond laser (Laser Export, TECH-1053) exhibited a pulse duration of 15 ns and a wavelength of 1053 nm, a maximum repetition rate of 4 kHz and a maximum pulse energy of 500 μ J. The picosecond laser (Edgewave, PX-200) had a pulse duration of 12 ps, a wavelength of 1064 nm and a maximum pulse energy of 600 μ J with a maximum repetition rate of 1 MHz. The interference diameter (d_i) in the ideal working position was estimated to be ~120 μ m for the nssetup and to ~250 μ m for the ps-configuration in the short axis (parallel to the interference fringes) using a beam camera system.

The texturing strategy followed a pulse-overlapping concept, where lines of pulses were fabricated by translating the sample parallel to the interference lines by high-precision motorized linear stages. The number of pulses (N) per spot was calculated from the pulse distance (p) and interference diameter as follows:

$$N = p/d_{\rm i}. (2)$$

In order to obtain long-range homogeneous structures, adjacent lines of pulses containing the interference pattern were fabricated by translating the samples perpendicular to the orientation of the interference fringes by the hatch distance (h_d) . The hatch distance was always set to an integer multiple (hatch factor, h_f) of the spatial period Λ so as to correctly overlap the interference maxima and minima of subsequent lines of pulses. The laser power was varied to obtain different fluence (Φ) values, which were calculated as the average fluence over the Gaussian beam profile. A schematic of the employed optical setup can be found in [18].

2.3 Surface topography characterization

The surface topographies were measured using a confocal laser-scanning microscope (CLSM, Keyence, VK-X3000) with a 50x and 150x magnification objectives. The surface roughness parameters were calculated using the self-developed Python library Surfalize [17] according to the ISO 25178 standard [9]. Moreover, periodic surface parameters such as the average peak-to-valley structure depth and aspect ratio were calculated according to the method proposed in [17] and implemented in Surfalize. The texture homogeneity was estimated using the Gini coefficient approach proposed by Lechthaler et al. [19]. High-resolution imaging of the surface textures was conducted using a scanning electron microscope (SEM) at 15 kV operating voltage (Jeol, JSM 6610LV).

2.4 Machine learning

In order to predict surface roughness and functionality, different machine learning models were applied on a dataset of textured surfaces. Before model training, the dataset underwent preprocessing to prepare it for regression analysis. Categorical variables, such as the pulse duration regime (nano- or picosecond), were encoded using one-hot encoding to represent them as binary vectors. Numerical features were standardized using z-score normalization to ensure all variables were on the same scale.

Each regression model was trained on a subset of the dataset and evaluated using appropriate performance metrics, such as mean squared error (MSE) and coefficient of determination (R^2). Cross-validation was employed to assess the models' generalization performance on unseen data. The hyperparameters of each model were fine-tuned using grid search with cross-validation to identify the optimal combination of hyperparameters that maximized predictive performance. All models were implemented using the scikit-learn library [20] in Python. Five models were selected to compare their performance when trained on the dataset: gradient boosting machines (GBM), multi-layer perceptron (MLP), support vector machines (SVM), random forest regressors and k-nearest neighbors (kNN).

3. Results and Discussion

In total, 610 different line-like textures were fabricated using the DLIP technique. Both pico- and nanosecond DLIP was used and the period Λ was varied between 4 and 12 μ m. The structure depth was varied by adjusting the process parameters such as the hatch distance, the number of pulses and pulse fluence (see experimental section). An overview of all textured samples is given in Table 1.

Table 1 Overview over different textures.

Pulse duration	Texture type	Spatial periods (1)	Number of textures
15 ns	Lines	4	105
		5	25
		6	50
		7	25
		8	25
10 ps	Lines	4	25
		6	50
		8	25
		10	25
		12	25

All fabricated topographies were measured using a CLSM and analyzed using Surfalize. For this purpose, the topographies are leveled and filtered with low-pass filter at a cutoff wavelength of $0.8 \, \mu m$. In a batch operation, all available roughness parameters from ISO 25178 implemented in Surfalize, as well as the structure depth (d), aspect ratio (AR) and texture homogeneity (H) were computed.

The difference of the surface topographies obtained with nano- and picosecond DLIP can be observed in Figure 1, which shows two produced line-like structured surfaces with a spatial period of 8.0 µm and a structure depth of approximately 4 µm. The nanosecond structure features a single-scale topography with protrusions that are caused due to the melting-dominated nanosecond material interaction [21]. The picosecond DLIP structured surface exhibits a more uniform depth modulation that more closely corresponds to the sinusoidal intensity distribution of the interference pattern. This is likely related to the reduced melt pool and increased direct evaporation during picosecond DLIP [22]. More differences between the pulse durations can be observed through different roughness parameters from ISO 25178 [9].

For instance, the measured skewness S_{sk} of the ns-DLIP surface was 0.50 μm^3 , indicating a stronger distribution of material towards the upper parts of the surface. In case of the ps-DLIP texture, a close to equal distribution with a value of -0.06 μm^3 was calculated. On the other hand, the surfaces exhibit a very close match of the developed surface area S_{dr} with a value of ~167%.

For each spatial period, one or multiple matrices of textures were fabricated, which consist of a variation of the laser fluence and number of pulses. Figure 2 shows the analysis of such a matrix on the example of a nanosecond process with a spatial period of $8.0~\mu m$ and a hatch distance of $32~\mu m$. Using Surfalize, both the structure depth (Figure 2a) and the pattern homogeneity (Figure 2b) were evaluated and plotted as a false color heatmap. It can be observed that the structure depth increased predominantly with the number of pulses and only slightly with increasing fluence. The largest texture depth of approximately $7~\mu m$ was generally observed for the highest number of pulses (14) and a relative high laser fluence of $1.47~J/cm^2$.

On the other hand, the homogeneity follows a different trend. It increases initially with increasing fluence and number of pulses, but sharply reduces again towards the maximum number of pulses and fluence in the upper right (see Figure 2b). A region of optimal homogeneity is visible around the center region (1.38 J/cm², 8 pulses) as well as lower fluence and high number of pulses. The origin of the different homogeneity values can be understood from the confocal images in Figure 2c-e corresponding to datapoints in the lower left, center and upper right of the matrix. For low number of pulses and fluence, the initial surface roughness still contributes significantly to the topography in the form of randomly distributed lines perpendicular to the DLIP topography. In the center, the DLIP process has removed the initial roughness, and the structures are well defined, leading to homogeneity values above 0.90. However, in the upper right region large number of pulses and high

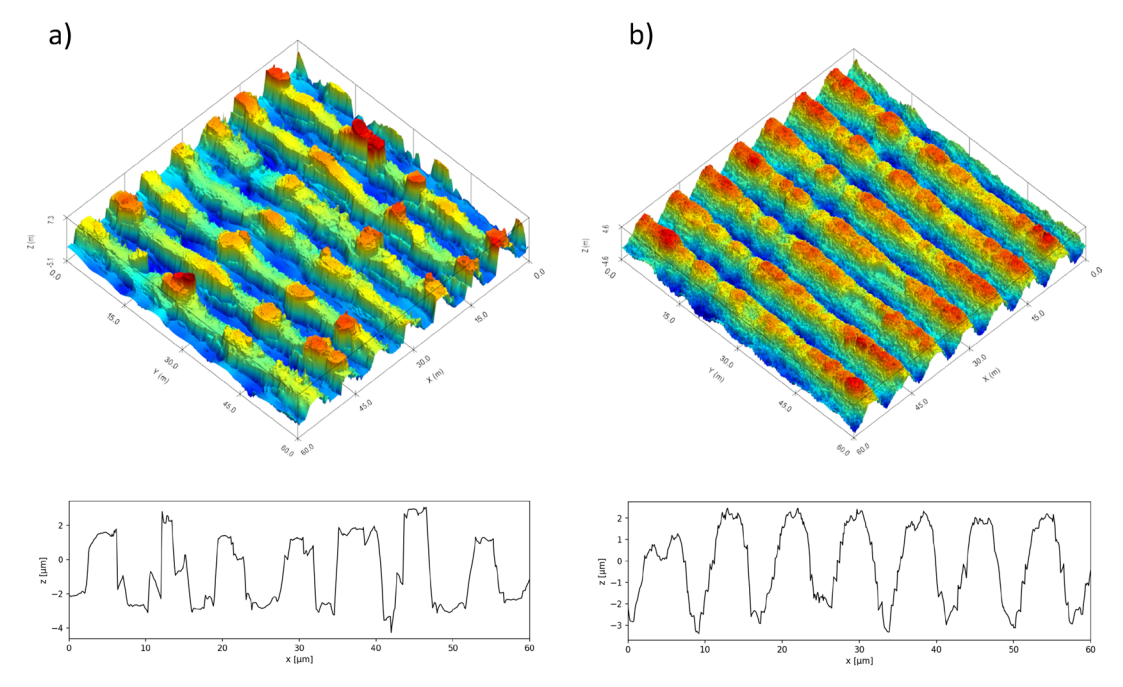


Fig. 1 Comparison of confocal measurements and profiles of a) ns-DLIP and b) ps-DLIP surface textures with a period of 8 μ m and an average depth of approximately 4 μ m.

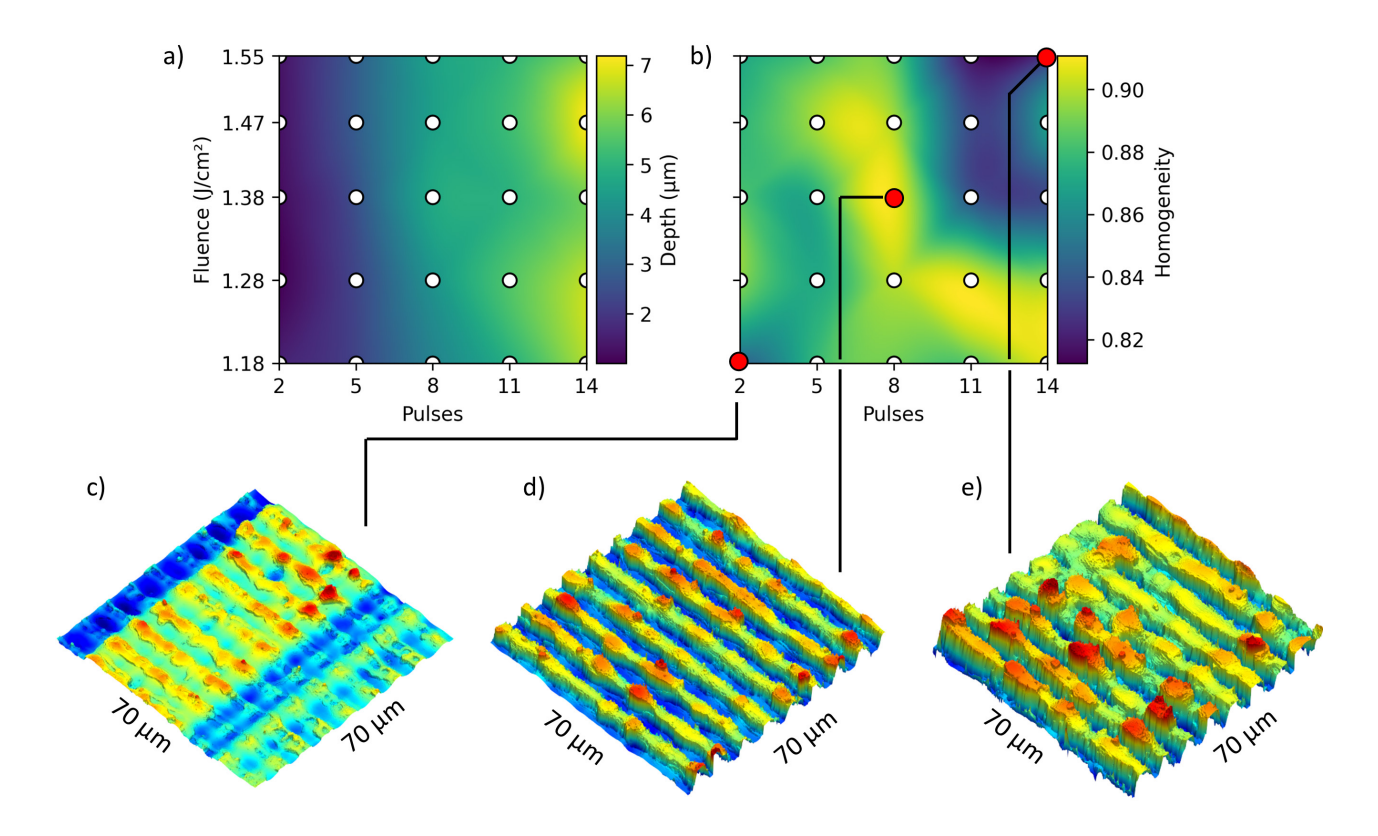


Fig. 2 Peak-to-valley (a) structure depth and (b) homogeneity as a function of fluence and number of pulses for DLIP textures fabricated with a nanosecond laser and a spatial period of 8 μm and a hatch distance of 32 μm. Confocal measurements of three different surfaces (c-e) exemplify the difference in morphology in terms of depth and homogeneity for different parameter combinations, where the central topography fabricated with 8 pulses and a fluence of 1.38 J/cm² features the highest homogeneity.

laser fluence), the texture starts to be characterized by melting due to heat accumulation, which results in randomly distributed protrusions and localized filling of the structure valleys by molten material, contributing to a more inhomogeneous surface.

To predict the resulting topography in terms of its characteristic roughness parameters from ISO 25178 as well as depth, aspect ratio and homogeneity, five different machine learning models (RFR, GBM, MLP, SVM, KNN) were trained on the topographical and laser parameters. The best fit plots for each model on the example of the arithmetic mean height (S_a) are shown in Figure 3, ordered by best to worst fit quality as measured by both MSE and R^2 . As it can be observed, the RFR results in a highly accurate prediction

with an R^2 of 0.93, closely followed by the GBM with an R^2 of 0.92. The MLP also performs well, but less accurate with an R^2 of 0.83. On the other hand, SVM and KNN only exhibit moderate predictive accuracy with R^2 values of 0.67 and 0.57, respectively, with predictions deviating significantly in the larger roughness range above 1 μ m.

This result can be explained by the robustness of RFR and GBM in regards to noisy data and their excellent ability to handle nonlinear relationships [23]. These are characteristics well suited to predict the complex relationship between roughness parameters and laser process parameters, which are known to follow nonlinear relationships [10]. On the other hand, SVN and KNN can struggle with non-linearities and noisy data [23].

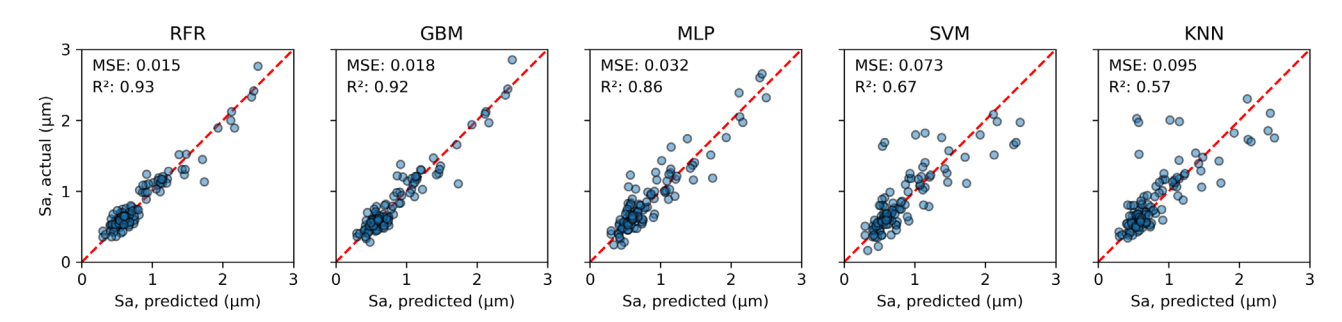


Fig. 3 Best fit plots showing the relationship between the actual and predicted values on the example of the arithmetic mean height (S_a) when using the five different models (RFR, GBM, MLP, SVM, KNN). The RFR achieves the best predictive accuracy with a coefficient of determination R^2 of 0.93.

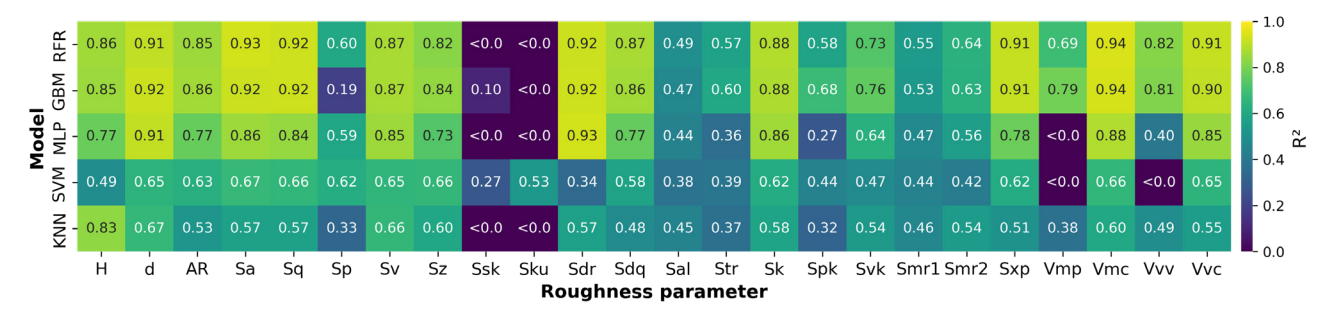


Fig. 4 Heatmap of the coefficient of determination (R^2) as a measure of model fit quality for all five investigated models and all investigated roughness parameters. The models are ordered from best to worst average performance.

Figure 4 shows the performance of the five investigated machine learning models in terms of the resulting coefficient of determination R^2 across all roughness parameters calculated by Surfalize, including the available ISO 25178 parameters as well as the self-defined parameters depth, aspect ratio and homogeneity. The models are sorted from best to worst performance averaged over all parameters, resulting in the same order as already observed for the arithmetic mean height in Figure 3. Moreover, it can be observed that the amplitude related parameters such as most height parameter family from ISO 25178 (Sa, Sq, Sp, Sv, Sz) as well as the depth and aspect ratio are very predicted with comparatively high accuracy by all models.

Similarly, the homogeneity was predicted very well by all models except SVM. This suggests that there is a clear relationship between the laser process parameters and these aspects of the resulting topography. On the other hand, the models for predicting $S_{\rm sk}$ and $S_{\rm ku}$ almost exclusively reached negative R^2 values, which indicates an extremely poor predictive performance (worse than predicting the mean of the dataset in all instances). This could be related to inappropriate feature engineering or too small datasets for this type of

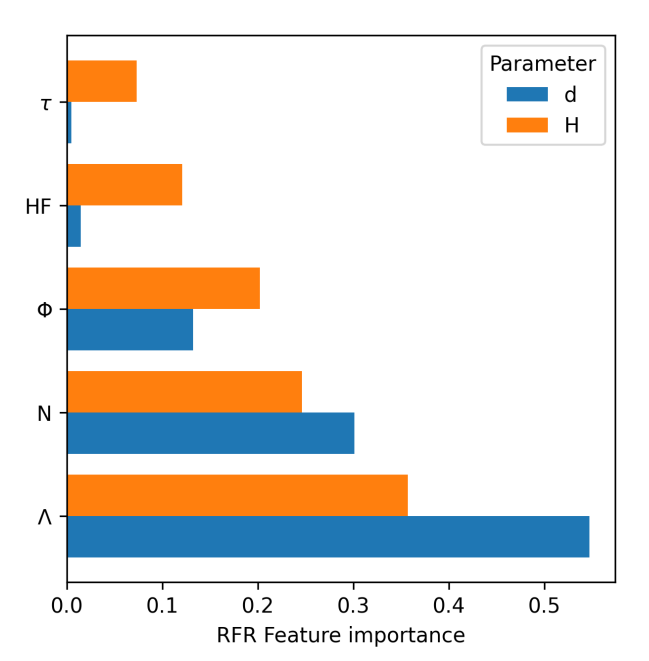


Fig. 5 Feature importance of the laser parameters extracted from trained RFR model for the structure depth d ($R^2 = 0.91$) and homogeneity H ($R^2 = 0.86$).

parameter. However, it is worth noting that S_{sk} and S_{ku} depend on the amplitudes third and fourth power, respectively, and are thus quite susceptible to small changes in the morphology. A typical distribution for S_{ku} for a matrix as shown in Figure 2, which follows a clear trend in depth and homogeneity, can typically feature an apparently random distribution of S_{sk} and S_{ku} , which indicate the skewness and kurtosis of the structure. Therefore, there might simply not be a direct relationship between the laser parameters and the values of the skewness and kurtosis, which might rather depend on random processes such as local melt agglomerations.

In contrast to the the amplitude quantities, the functional parameters are predicted only with moderate accuracy by RFR and GBM, with R^2 values generally above 0.5, except for the core height Sk. The significantly better predictive performance for the core height is likely to be related to its high degree of correlation with the amplitude related parameters. Moreover, the definition of S_k makes it particularly robust against outliers, reducing noise and influence of random processes in the structure formation on the distribution of Sk values. On the other hand, quantities such as the reduced peak height Spk and reduced dale height Svk can be quite different depending on the formation of localized melt protrusions on the surface, which can even vary depending on the selected measurement area. The functional volume parameters (V_{mp}, V_{mc}, V_{vv}, V_{vc}), which are also defined on the Abbott-Firestone curve, are much more accurately predicted by RFR and GBM compared to the regular functional parameters.

Lastly, successfully trained models such as the RFR were employed to estimate the importance of the process parameters to the target topographical quantity. Figure 5 shows the feature importance on the example of a RFR trained on the relationship between the laser process parameters and the structure depth (in blue) as well as the homogeneity (in orange). As can be observed, the dominant predictor of both parameters is the structure period, which at first glance might seem counterintuitive. However, in the case of DLIP, this can be explained by as follows: due to the thermal diffusion between two adjacent interference maxima in the material, the material can only withstand a certain amount of cumulated fluence before extensive melting reduces structure homogeneity and depth [24]. For metals treated with nanosecond pulses (10-20 ns), the thermal diffusion length can lie around ~1 μm [24]. Therefore, larger spatial periods also generally allow for greater structure depths [25], making the period the most important determinant for the achievable structure depth. Moreover, both the hatch factor and laser

fluence play a significant role in determining homogeneity than structure depth. This is likely related to the emergence of a second modulation for too large hatch distances [25], adversely impacting homogeneity, and high fluences leading to increased melting.

4. Conclusions

In this work, we show how the self-developed Python library Surfalize and machine learning can be employed to predict surface roughness of DLIP-textured stainless steel specimens. After fabricating more than 600 different DLIP textures with different laser parameters, the measured topographies were evaluated by the self-developed Python library Surfalize, in terms of standardized roughness parameters and self-defined features such as structure depth and homogeneity. Using different machine learning algorithms, we demonstrated the possibility to predict topographic characteristics from the laser parameters and extract feature importance. Notably, we showed that random forest regressors and gradient boost machines resulted in high predictive accuracy for a wide range of settings, whereas support vector machines and k-nearest neighbors did not prove to be suitable for this task. Lastly, this work demonstrated the efficacy of the Surfalize to integrate surface roughness analysis into the Python machine learning toolchain.

Acknowledgments

We thank Eric Gärtner for providing the stainless-steel samples and Richard Chukwudi Okafor for his help in texturing the samples. This research was partially funded by the German Federal Ministry for Economic Affairs and Climate Action (BMWK) within the Promotion of Joint Industrial Research Programme (IGF) due to a decision of the German Bundestag. It was part of the research project 21934 BR by the Association for Research in Precision Mechanics, Optics and Medical Technology (F.O.M.) under the auspices of the German Federation of Industrial Research Associations (AiF).

References

- [1] A. Cunha, A. P. Serro, V. Oliveira, A. Almeida, R. Vilar, and M.-C. Durrieu: Appl. Surf. Sci., 265, (2013), 688
- [2] C. Liu, S. Tong, Y. Yue, H. Wang, J. Song, Y. Li, Q. Wang, and Z. Wang: Colloids Surf. Physicochem. Eng. Asp., 688, (2024), 133648
- [3] A. Hariharan, P. Goldberg, F. Schell, U. Hempel, F. Striggow, M. Hantusch, M. Medina-Sánchez, A. F. Lasagni, and A. Gebert: Adv. Funct. Mater., (2023), 2310607
- [4] K. O. Böker, F. Kleinwort, J.-H. Klein-Wiele, P. Simon, K. Jäckle, S. Taheri, W. Lehmann, and A. F. Schilling: Materials, 13, (2020), 3526
- [5] H. Heffner, M. Soldera, and A. F. Lasagni: Adv. Eng. Mater., 24, (2022), 2200266

- [6] N. Charipar, R. C. Y. Auyeung, H. Kim, K. Charipar, and A. Piqué: Opt. Mater. Express, 9, (2019), 3035
- [7] Y. Xu, Z. Li, G. Zhang, G. Wang, Z. Zeng, C. Wang, C. Wang, S. Zhao, Y. Zhang, and T. Ren: Tribol. Int., 134, (2019), 352
- [8] S. Rung, K. Bokan, F. Kleinwort, S. Schwarz, P. Simon, J.-H. Klein-Wiele, C. Esen, and R. Hellmann: Lubricants, 7, (2019), 43
- [9] DIN ISO 25178-2:2012, Geometrical product specifications (GPS) - Surface texture: Areal; Part 2: Terms, definitions and surface texture parameters (ISO 25178-2:2012). 2012.
- [10] B. Voisiat, A. I. Aguilar-Morales, T. Kunze, and A. F. Lasagni: Materials, 13, (2020), 200
- [11] M. El-Khoury, B. Voisiat, T. Kunze, and A. F. Lasagni: Materials, 13, (2020), 4101
- [12] T. Steege, G. Bernard, P. Darm, T. Kunze, and A. F. Lasagni: Photonics, 10, (2023), 361
- [13] L. Moles, I. Llavori, A. Aginagalde, G. Echegaray, D. Bruneel, F. Boto, and A. Zabala: Tribol. Int., 200, (2024), 110067
- [14] Y. Cao, C. Chen, S. Xu, R. Zhao, K. Guo, T. Hu, H. Liao, J. Wang, and Z. Ren: Addit. Manuf., 91, (2024), 104341
- [15] K. Li, R. Ma, Y. Qin, N. Gong, J. Wu, P. Wen, S. Tan, D. Z. Zhang, L. E. Murr, and J. Luo: J. Mater. Process. Technol., 318, (2023), 118032
- [16] S. L. Sing, C. N. Kuo, C. T. Shih, C. C. Ho, and C. K. Chua: Virtual Phys. Prototyp., 16, (2021), 372
- [17] F. Schell, C. Zwahr, and A. F. Lasagni: Nanomaterials, 14, (2024), 1076
- [18] F. Schell, A. Hariharan, P. Goldberg, R. Baumann, E. Jäger, A. Gebert, C. Zwahr, and A. F. Lasagni: J. Laser MicroNanoengineering, 17, (2022), 199
- [19] B. Lechthaler, C. Pauly, and F. Mücklich: Sci. Rep., 10, (2020), 14516
- [20] F. Pedregosa, G. Varoquaux, A. Gramfort, V. Michel, B. Thirion, O. Grisel, M. Blondel, P. Prettenhofer, R. Weiss, V. Dubourg, J. Vanderplas, A. Passos, D. Cournapeau, M. Brucher, M. Perrot, and E. Duchesnay: J. Mach. Learn. Res., 12, (2011), 2825
- [21] B. N. Chicbkov, C. Momma, and S. Nolte: 7
- [22] P. Goldberg, A. Hariharan, F. Schell, M. Hantusch, M. O. Cichocka, N. Pérez, A. Voß, L. Giebeler, V. Hoffmann, C. Zwahr, A. F. Lasagni, and A. Gebert: Corros. Sci., 219, (2023), 111230
- [23] T. Hastie, R. Tibshirani, and J. Friedman: The Elements of Statistical Learning. New York, NY: Springer New York, 2009.
- [24] A. Lasagni, M. D'Alessandria, R. Giovanelli, and F. Mücklich: Appl. Surf. Sci., 254, (2007), 930
- [25] A. I. Aguilar-Morales, S. Alamri, T. Kunze, and A. F. Lasagni: Opt. Laser Technol., 107, (2018), 216

(Received: July 2, 2025, Accepted: September 13, 2025)